Engineering Structures 179 (2019) 174–188

Contents lists available at ScienceDirect

Engineering Structures

journal homepage: www.elsevier.com/locate/engstruct

A non-emulative moment connection for progressive collapse resistance in precast concrete building frames

Spencer E. Quiel*, Clay J. Naito, Corey T. Fallon

Department of Civil and Environmental Engineering, Lehigh University, Bethlehem, PA 18015, USA

ARTICLE INFO

Keywords:
Progressive collapse
Precast concrete
Moment connection
Experimental testing

ABSTRACT

This paper documents the experimental development of a new spandrel-to-column moment connection detail for progressive collapse resistance in precast concrete building frames. This study focuses on a 10-story prototype precast concrete frame building with perimeter special moment frames (SMF) that are subjected to a ground-floor column removal. The experimental subassembly represents a spandrel-to-column connection on the perimeter SMF near the middle of the building face (i.e. not at the corners). The connection is non-emulative and utilizes unbonded high-strength steel post-tensioning (PT) bars which pass through ducts in the column and are anchored to the spandrels via bearing plates. The proposed design strives for construction simplicity, avoids field welding and/or grouting, and maximizes ductility by allowing the high strength steel bars to act as structural "fuses" when yielding. A full-scale quasi-static pushdown test is performed on two variants of the proposed connection: one with higher moment-rotation capacity and limited ductility, and another with lower capacity and higher ductility. The results show that the connection can reliably achieve its design yield capacity, performs well under service level demands, and can achieve moderate-to-high ductility. The experimental results are then applied to a system-level computational model of the prototype building frame under a column removal scenario. The results of a nonlinear dynamic analysis demonstrate that the system can arrest progressive collapse in the event of a single column loss scenario when either variant of the proposed connection is considered.

1. Introduction

Progressive collapse of a structural system occurs when localized failure of a primary load-bearing element leads to a larger, more widespread collapse of adjoining portions of the structure. This type of collapse, which can affect multiple floors and/or multiple bays up to the entire structure, is regarded as a disproportionate response to the initial local damage. To prevent a chain reaction of structural failure in elements surrounding the local damage, a structural system must be able to redistribute its loads to bridge over the damaged areas without suffering a catastrophic collapse. In current design guidelines, the initial local failure for framed structures is typically identified as the significant loss of load-carrying capacity by a single primary vertical load-bearing element (i.e. a column). The sudden loss of a column in a framed structure has two primary effects: (1) increased span length for horizontal elements (i.e. beams) that were previously supported by the column, and (2) inertial amplification of the associated gravity forces as the structure tries to reestablish equilibrium. Both effects result in increased demands on the undamaged portions of the structure. Because of the increased demands, two primary progressive collapse mechanisms may occur: (1) flexural or shear failure of the horizontal elements (beams or girders) located above the damaged column, or (2) overload of the vertical elements (columns) located adjacent to the damaged column due to load redistribution. Other mechanisms involving the secondary structural elements (e.g. the failure and/or detachment of the floor system) may also occur but are not considered in this study.

The ability of a structure to resist a disproportionately large collapse due to localized damage has become a topic of increasing concern within the building community in the wake of structural collapses worldwide over the last half century. Design concepts for progressive collapse resistance have been developed in response to these events, which include the 1968 collapse at Ronan Point in the UK [1] and the progressive collapse of the Murrah Federal Building resulting from the 1995 Oklahoma City bombing [2]. These approaches include (1) "tying" elements together via added reinforcement or stronger connections to improve structural continuity, (2) designing the structure with alternate load paths around locations of likely damage, and (3) designing structural systems to fail in a ductile (i.e. gradual) rather than brittle (i.e. sudden) manner. The alternate load path approach in

* Corresponding author.
E-mail address: squiel@lehigh.edu (S.E. Quiel).

https://doi.org/10.1016/j.engstruct.2018.10.027
Received 31 May 2018; Received in revised form 7 September 2018; Accepted 12 October 2018

particular has become the centerpiece of the two leading guideline documents for progressive collapse resistant design that are published by the U.S. Government [3,4]. According to these current standards, progressive collapse resistant design via the Alternate Path Method (APM) is implemented by removing columns one at a time in one-story lengths from the structural frame at several locations to simulate the local damage. The loads supported by the removed element(s) must then be redistributed to the surrounding structure to prevent collapse. To date, the construction of progressive collapse resistant buildings has typically consisted of either structural steel or cast-in-place concrete frames that have been strengthened and detailed to bridge loads over areas of potential damage. The current standards provide detailed guidance and examples for the implementation of these structural system types to resist progressive collapse based on the results of numerous research studies. Seismic detailing is often adapted to help the structure redistribute its loads.

Implementation of these provisions to achieve progressive collapse resistance invariably leads to an increase in the cost of construction. Recent industry studies have suggested that implementation of progressive collapse resistance to multi-story buildings can increase to the cost of the structural system up to 30% [5] and the overall cost of the building by up to 3% [6]. Therefore, progressive collapse resistant design has typically been reserved for structures that are either more susceptible to extreme loading (due to their location, use, or occupancy) or serve a critical function (such as hospitals or government facilities). The higher cost of construction in response to a low probability yet high consequence event poses a significant challenge to building owners, including both private companies and government agencies, in the current economic and fiscal environment.

To reduce cost, there has been increasing interest in using structural systems composed of prefabricated concrete elements to achieve progressive collapse resistant design. Precast concrete frames offer significant cost savings and construction time reductions versus cast-in-place concrete or structural steel framed systems by fabricating all elements off site and then assembling the frame using simplified connection details. Design methodologies and details for earthquake resistant precast concrete frames [7] have gained acceptance in the industry and have been implemented in seismically active regions. However, current progressive collapse criteria documents provide little guidance regarding the design approach or connection detailing to be used for this construction type. Structures comprised of precast concrete framing are also perceived as less robust since prefabricated elements are typically assembled using connections that cannot transfer bending between elements and therefore cannot create continuous spans (which are needed to bridge over damaged areas). A lack of published research presents a significant barrier to the use of this cost-effective structural system to provide greater levels of structural safety.

A number of studies have specifically addressed the structural integrity of precast concrete systems [8–13], but few have focused on the response of total precast systems (i.e. without emulative connections that are cast-in-place or grouted) to column loss. The most notable effort was led by NIST [14] and focused on the progressive collapse resistance of a total precast concrete frame designed for seismic resistance [15]. The system was composed of deep precast concrete spandrel beams attached to precast concrete columns. The standard connection detail consisted of embedded steel plates and welded reinforcement bars in the spandrel that were attached to the column through welded steel jumper plates. That study concluded that typical welded precast concrete seismic moment frame connection details may not be able to achieve their design strength or significant rotational ductility in response to a single column removal scenario, which represents the majority of progressive collapse design applications.

The goal of the study presented in this paper is to develop a connection detail that provides predictable and reliable flexural capacity in response to the column loss scenario in a realistic precast building frame. The prototype building system considered in this study is the same 10-story design that was developed by Kim et al. [15] and used in the study by Main et al. [14]. The proposed connection consists of L-shaped spandrel beams that are connected through the column by unbonded high-strength (1034 MPa (150 ksi)) steel post-tensioning (PT) bars. The proposed design strives for construction simplicity, avoids field welding and/or grouting, and maximizes ductility by allowing the high strength steel bars to act as structural "fuses." An experimental test program was performed to demonstrate that adequate strength and ductility can be achieved from the newly proposed connection detail. Specifically, a full-scale quasi-static pushdown test was performed on two variants of the proposed connection: one with higher moment-rotation capacity and limited ductility, and another with lower capacity and higher ductility. The objective of the experimental study is to show that the connection can reliably achieve its design yield capacity, performs well under service level demands, and can achieve moderate-to-high ductility. The experimental results are then applied to a system-level computational model of the prototype building frame under a removal scenario. The results of a nonlinear dynamic analysis are used to demonstrate that the system can arrest progressive collapse in the event of a single column loss scenario.

2. Prototype building and modified moment connection design

2.1. Prototype system

The prototype system is a total precast concrete office building comprised of an exterior moment frame, which encompasses the full perimeter of the structure [15]. The plan and elevation views of the prototype system are shown in Fig. 1. The plan layout is square with dimensions of 45.7 m × 45.7 m (150 ft × 150 ft). The typical story height is 3.96 m (13 ft) except for the first story which is 4.57 m (15 ft). The location of the structure is assumed to be Seattle, Washington, which requires a special moment frame (SMF) lateral force resisting system at Seismic Design Category D. The floor system is comprised of double-T beams and topped with 8.89 cm (3.5 in.) of concrete on average. The interior frame is designed to resist gravity load only and does not contribute to the building's lateral force resistance.

The prototype building system was designed for ASCE 7-05 Occupancy Category II [15]. Gravity loads included the structural self-weight, superimposed dead load of 0.479 kPa (10 psf), floor live load of 4.79 kPa (100 psf), and roof live load of 1.20 kPa (25 psf) – live load reduction was considered in accordance with ASCE 7-05 [16]. The concrete members were designed in accordance with ACI 318-05 [17] with the spandrel beams based on the PCI Design Handbook [18]. Normal weight concrete, 23.6 kN/m^3 (150 lbf/ft^3) was used with a design compressive strength of 41.4 MPa (6000 psi) for the precast elements and 27.6 MPa (4000 psi) for the concrete topping. Grade 60 reinforcement (i.e., minimum yield strength of 414 MPa (60 ksi)) was used in all precast elements.

2.2. Proposed connection design

The moment connection considered in the original design of the prototype system by Main et al. and Kim et al. [14,15] was comprised of two steel link plates that were located 152 mm (6 in.) from the top and bottom of the 1.57 m (62 in.) deep spandrel and welded to embedded plates in both the column and the beam. The embedded plates are anchored to the spandrel by three #36 (#11) steel bars that are welded to the opposite face and cast into the spandrel. The approximate factored yield moment is 1428 kN-m [or (0.9)(3.0)(1.56 in.^{2})(60 ksi)(50 in.)(1 ft/12 in.) = 1053 kip-ft] and expected yield moment of 1586 kN-m (1170 kip-ft). This strength calculation is conservative since the moment arm is assumed to span from the center of the top reinforcement group to the center of the bottom reinforcement group. Experimental tests by Main et al. [14] on these connections did not achieve the expected yield capacity – instead, fracture of reinforcement

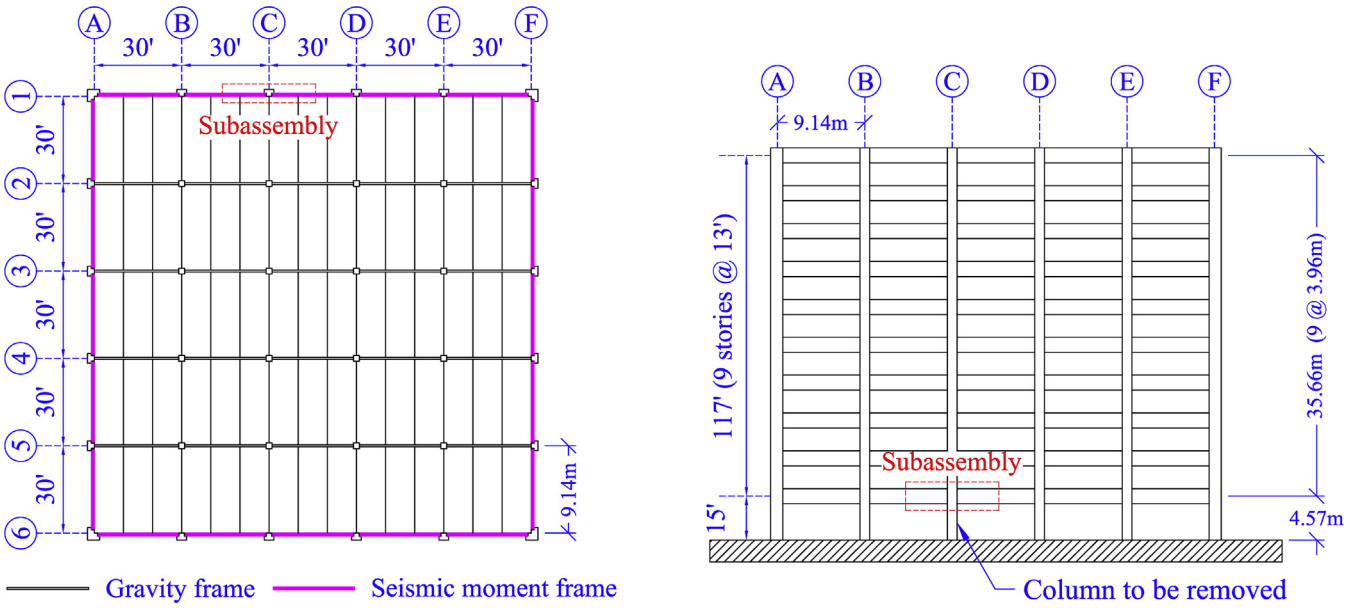

Fig. 1. Prototype building system (plan and elevation).

was observed at approximately 75% of the expected yield capacity, though additional post fracture strength was achieved through arching action in the frame. The connection failed in a brittle mode due to the presence of rebar welds and eccentricity in the load path through the spandrel beam to column connection [14].

The focus of this study is the development of a new spandrel-to-column moment connection in the exterior moment frame which can form a ductile flexural mechanism and withstand progressive collapse in the event of exterior column damage. The connection design embraces the total precast concept by eliminating grout and wet casting, which maintains the constructability advantages of these systems. The proposed detail is designed to achieve comparable yield moment capacity to that of the aforementioned seismic connection that was designed for the original prototype. Since eccentricities are difficult to eliminate entirely in precast concrete connections, the primary consideration in the development of the proposed connection is the elimination of welds in the flexural load path. The design concept is illustrated in Fig. 2. Unbonded high strength steel (1034 MPa or 150 ksi) PT bars pass horizontally through the column as well as anchorage blocks on the interior face of each spandrel. The ends of the PT bars are anchored with nuts on bearing plates at the far end of the anchorage blocks. U-shaped plastic shims are placed between the column and each anchorage block around the PT bars. The spandrels rest on bearing pads in a pocketed column, thus providing shear transfer in bearing. Two threaded torsion rods pass through blockouts in the column in the out-of-plane direction and are connected perpendicularly to embeds in the spandrel's interior face within the column pocket. The other end of these bars are anchored by nuts on bearing plates on the interior column face.

Two sizes of PT bars were used in this study: 46 mm (1–3/4 in.) diameter and 36 mm (1–3/8 in.) diameter. The bars conform to ASTM A722-15 [19] Type II (deformed) high-strength steel bars for prestressed concrete. These bars have a minimum tensile strength of 1034 MPa (150 ksi) and a minimum yield strength of 80% of the minimum tensile strength. Preliminary design capacity calculations are performed using a minimum moment arm of 1194 mm (47 in.), i.e., the center-to-center vertical distance between the bars. The actual moment arm, when the system reaches flexural capacity, will be longer when the top compression zones of the anchorage blocks bear on the column. The nominal yield moment of the 46 mm (1–3/4 in.) diameter and 36 mm (1–3/8 in.) bar assemblies is 1644 kN-m [(2.58 in.^{2})(120 ksi)(47 in.)(1 ft/12 in.) = 1213 kip-ft] and 1007 kN-m [(1.58 in.^{2})(120 ksi)(47 in.)(1 ft/12 in.) = 742.6 kip-ft], respectively. Factored design values are taken as 90% of the nominal yield moment. The moment capacity of the proposed assembly with the 46 mm (1–3/4 in.) bars is conservatively comparable to the original connection design by Kim et al. [15], which had an expected yield capacity of 1586 kN-m (1170 kip-ft). The smaller bar size was chosen as a lower capacity alternative that would experience increased plastic deformation and thus potentially offer a more ductile response.

The test specimens are designed to ensure that the spandrel-to-column flexural connection is the controlling nonlinear mechanism. The flexural and shear capacity of the spandrel, anchorage blocks, and column are over designed accordingly. The spandrel's anchorage blocks are also designed to act as bearing supports (or corbels) for double-T stems at the exterior frame. The geometry and reinforcement details are illustrated in Figs. 3 and 4.

3. Experimental setup

According to the current APM procedures for progressive collapse resistance design [3,4], the design basis damage scenario is the instantaneous loss of a single vertical load bearing element (i.e. a 1-story height of a column or portion of a wall). The elevation of the prototype system in Fig. 1 shows the location of the ground floor column that will be "damaged" and removed for this study. As previously mentioned, single column removal can lead to progressive collapse as a result of two potential mechanisms: (1) the adjacent undamaged columns are overloaded because of load redistribution from the removed column, or (2) a "zipper" type mechanism in which the girders or spandrels above the removed element form a flexural collapse mechanism. The first mechanism can be mitigated by appropriately sizing the columns to resist the redistributed loads. This study focuses on the second mechanism, which can be resisted when the spandrels and spandrel-to-column connections in the bays above the removal have adequate moment capacity and rotational ductility. The recommended gravity load combination under the collapse scenario is 1.2D + 0.5L, which is consistent with the "extreme load" combination in ASCE 7 [16,20]. When a column is suddenly removed, the loads supported by that column become amplified by dynamic downward inertial effects as the system attempts to achieve equilibrium. To resist these loads, the frame must redistribute these amplified loads to the neighboring elements,

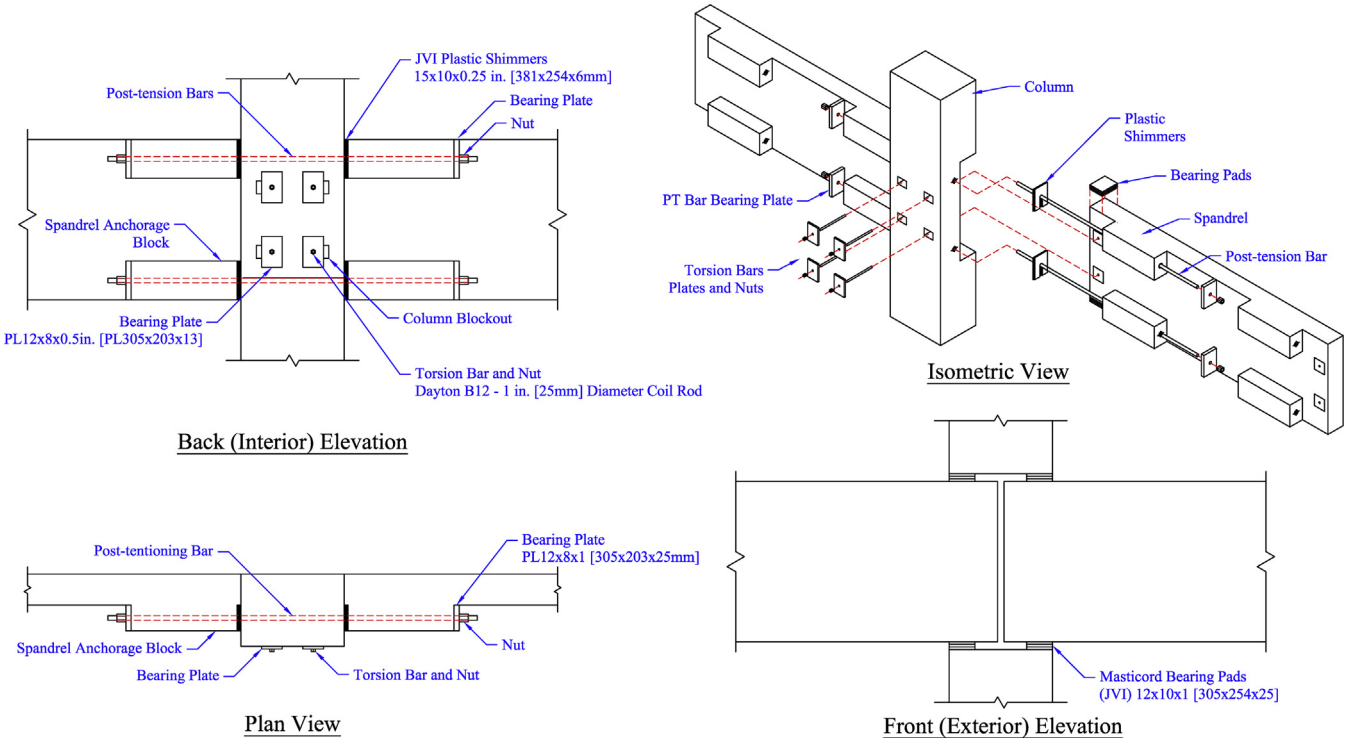

Fig. 2. Proposed column-to-spandrel connection concept.

often utilizing plastic flexural deformation in the horizontal framing above the removal.

The purpose of the experimental program is to assess the performance of the proposed connection assembly when subjected to this type of progressive collapse scenario. The tested subassembly for this study consists of a column segment above the removal and a

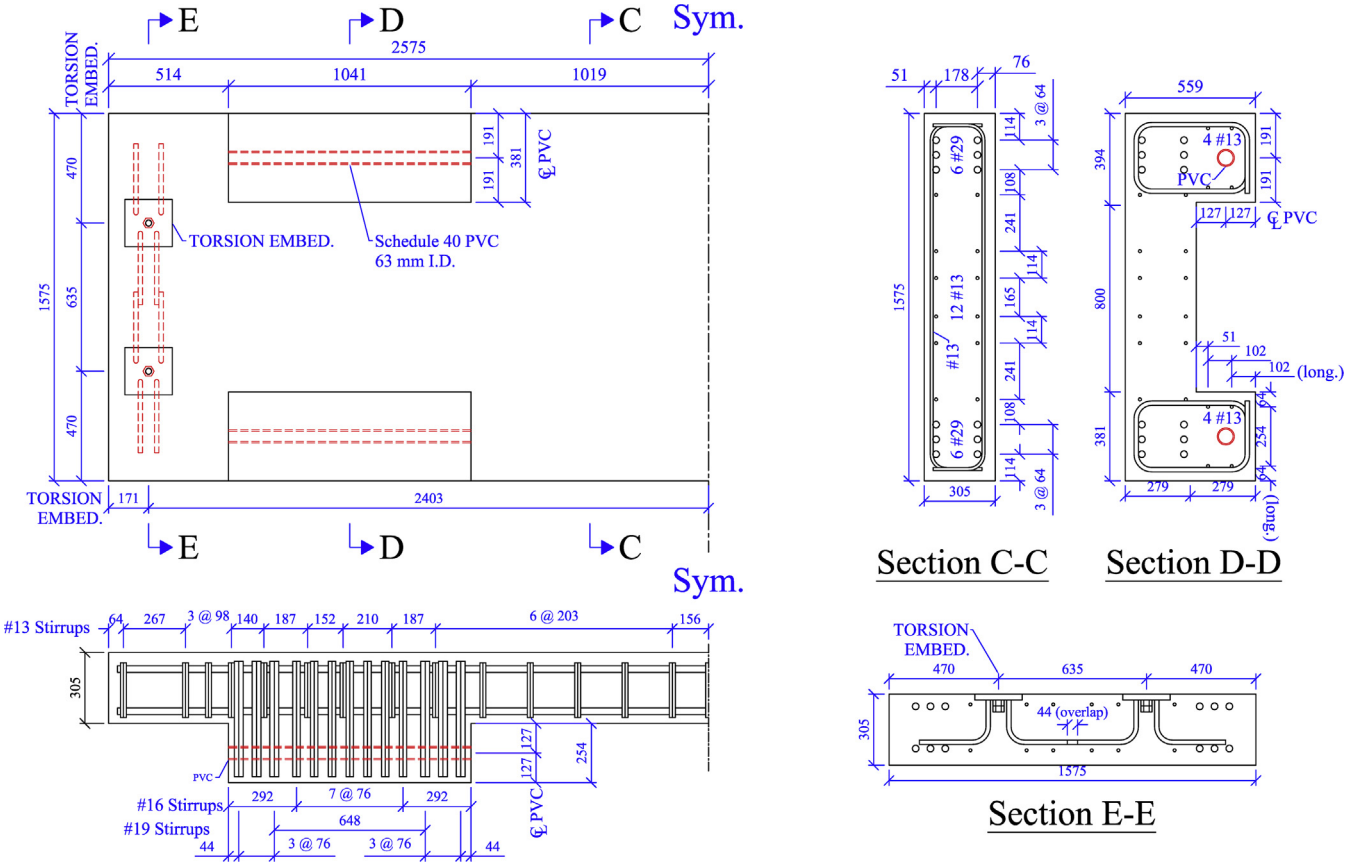

Fig. 3. Spandrel schematic details.

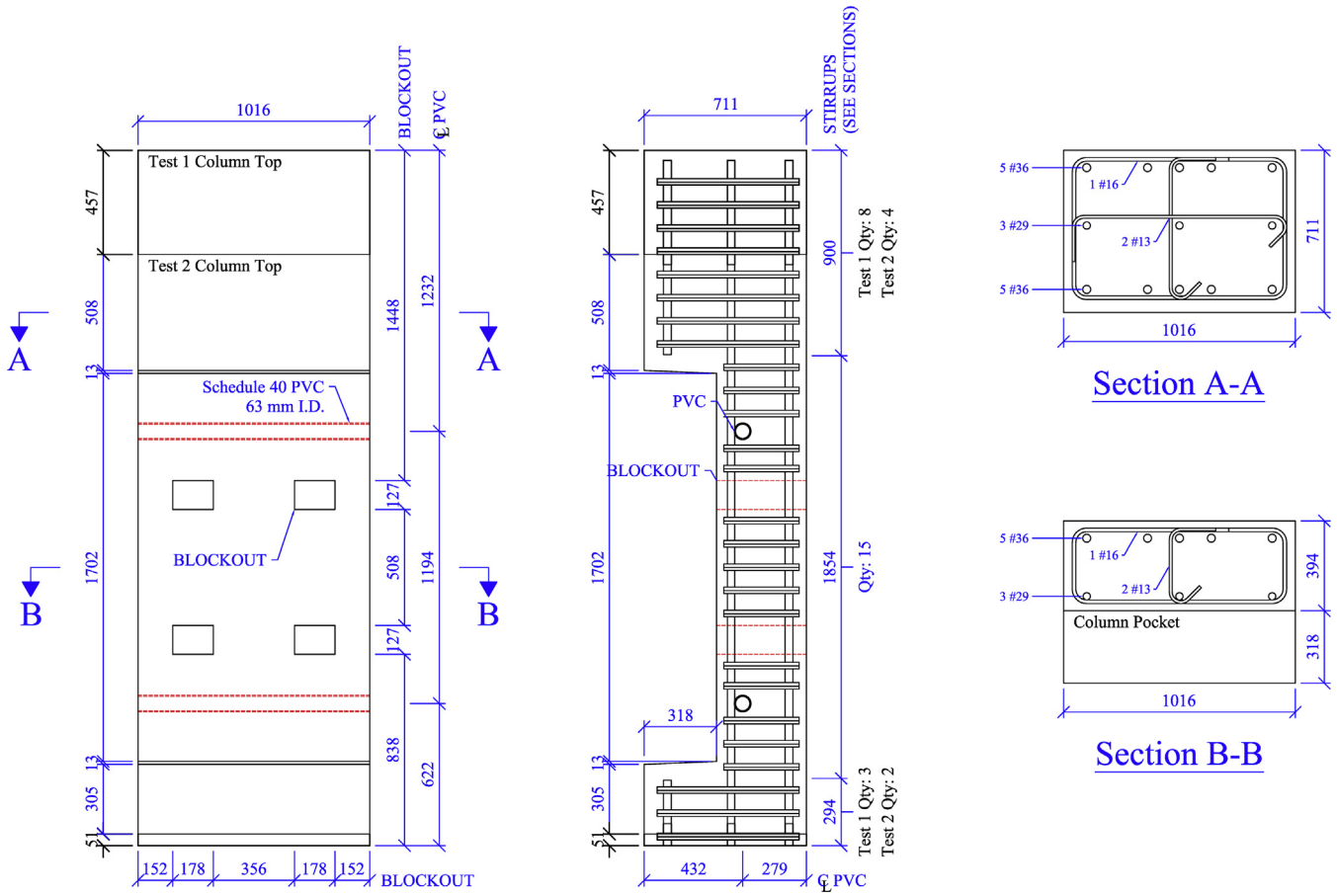

Fig. 4. Column schematic details.

symmetric portion of the beam span on either side of that column. All components in the subassembly are full scale, and the total span is designed to approximate the moment and shear demand under the removal scenario. To this end, the full two-bay span of the spandrels with the column removed is abridged by using a simply supported span between the two inflection points of the total span over the column removal. This approach almost halves the required span length for the subassembly as compared to the full two-bay span. Two point loads applied via actuators are used to impose the approximate moment and shear that would be generated from the uniform distributed load in the prototype. As shown in Fig. 5, the subassembly length is 9.78 m (384.9 in.) with point load application at 2.40 m (94.6 in.) from each support. Fig. 5 also shows that the moment and shear demands from the point loads on the subassembly are reasonably comparable with the demands expected under a uniform loading condition for the removal scenario in the actual frame.

3.1. Testing assembly

A 3D isometric view of the experimental assembly is shown in Fig. 6, and a schematic view is provided in Fig. 7. Load is applied with two hydraulic actuators mounted to cross beams. Pin and roller support conditions are achieved with loading carriages that are mounted to the spandrel. The pin end is bolted to the rocking plate to inhibit horizontal motion. The roller support utilizes a Teflon pad between the carriage and the rocker plate to allow horizontal movement. Similar load carriages are installed at the actuator-spandrel interface to ensure contact throughout the loading phase. The actuator loads and the end reactions are applied through the center of the rectangular spandrel section.

Eight steel skids are installed near the four interior columns (two on each column near the top and bottom of the spandrel depth) to restrain any potentially excessive out-of-plane torsion of the spandrel-to-column assembly during testing. The skids are comprised of steel angles with a welded nut, which receives a threaded rod whose end is welded to a bent skid plate. The threaded rod enables adjustment of the contact between the skids and the spandrel. Before the loading procedure begins, the threaded rods are extended such that the skids are almost in contact with the spandrel face. In this way, the skids can provide restraint for significant out-of-plane movement and minimize friction drag on the spandrel face.

Instrumentation consists of displacement transducers, tilt meters, load cells, and strain gages mounted on both the concrete surface and steel components. Details of the instrumentation locations and types are detailed in [21].

3.2. Material properties

A design concrete compressive strength of 41.4 MPa (6000 psi) was used for the precast elements. A standard precast concrete mix was used incorporating type III cement. The concrete compressive strength of the spandrels was measured in accordance with ASTM C39 [22] on each test day. Test 1 had compressive strength of 61.9 ± 2.9 MPa (8980 ± 420 psi), and Test 2 a compressive strength of 53.7 ± 5.4 MPa (7790 ± 780 psi). Grade 60 reinforcement (i.e., minimum yield strength of 414 MPa (60 ksi)) was used for all mild reinforcement in the test specimens. Both tests used ASTM A722-15 [19] Type II (Deformed) high-strength steel PT bars which have a specified minimum yield and tensile strength of 827 MPa (120 ksi) and 1034 MPa (150 ksi), respectively. Test 1 utilized 46 mm (1–3/4 in.) nominal diameter bars produced by Williams Form Engineering Corp., and Test 2 utilized 36 mm (1–3/8 in.) nominal diameter bars produced by Dywidag Systems International. Duplicates of each bar type were tested in

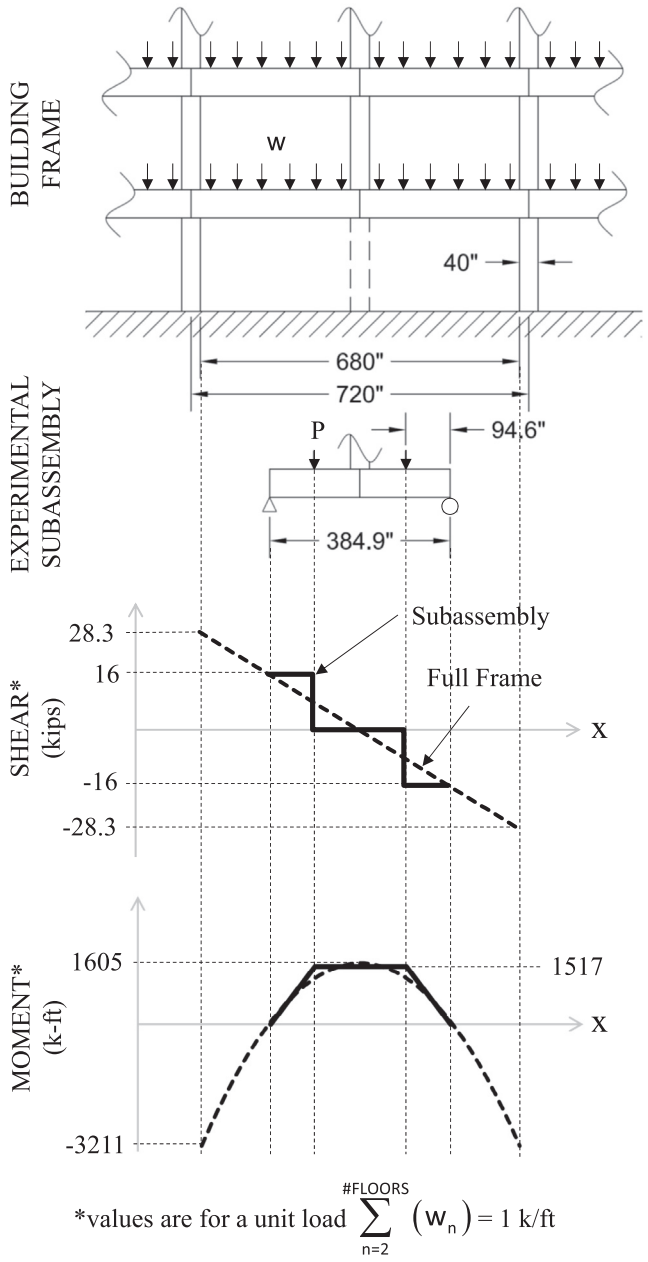

Fig. 5. Shear and moment mechanics of the experimental subassembly.

accordance with ASTM A370 [23], and the average yield (computed at a 0.2% offset) and ultimate strengths are summarized in Table 1. Elongation at maximum tensile strength was 4.64% for the 46 mm (1–3/4 in.) bars and 7.16% for the 36 mm (1–3/8 in.) bars. The lower bound moments at yield and ultimate (calculated earlier assuming a 47-in. moment arm between the bar locations) are updated here to represent an expected, unfactored value based on the material testing results.

A full description of the materials tested prior to the subassembly tests is provided in [21], which also includes compression testing of the plastic shims placed at the interface of the columns and the anchorage blocks on the spandrel. These plastic shims (Shimmers™) are made of an engineered copolymer plastic material (High Impact Polystyrene, or H.I.P.S.) were produced by JVI, Inc. Quasi-static compression tests of the shims showed an elastic stiffness of 1744 MPa (253 ksi) and a yield stress of 31.8 MPa (4.61 ksi).

3.3. Test procedure

Both tests were performed using the same 8-step procedure:

(1) The specimen is installed, and the spandrels are fastened to the column in a fully supported manner. The pin and roller carriages are tightened to develop the end supports. The actuator carriages are left loose so that the actuators will not contact the spandrels until later in the procedure. The spandrels are supported on temporary braces spanning between the interior frame columns, and a temporary support was used under the column. This position represents a fully shored condition in which the assembly supports no loads.
(2) All spandrel to column connections are made. This includes the flexural through bars and the out-of-plane torsion bars that attach the spandrel to the face of the column. Connections are made snug-tight (i.e. there is negligible tension in these bars at this stage).
(3) All instrumentation is connected, and the data acquisition is started.
(4) The through bars are tightened to approximately 13.3 kN (3 kips) using a wrench and monitoring of the axial strain gages on the bars. The torsion bars are tightened by wrench to approximately 71.2 kN (16 kips) tension through monitoring of their strain gages.
(5) An Enerpac hydraulic jack is placed under the stub column to provide an upward force to allow the removal of the temporary supports. Uplift pressure is initiated and monitored until the pressure multiplied by the piston area equals the tributary weight. This position represents the self-weight flexural condition when the column is still intact, just prior to removal. At this position, the specimen is no longer in contact with all temporary supports, which are removed.
(6) The jack is then unloaded, allowing for the application of the test assembly self-weight to the spandrel-to-column connection. This position represents the first load transition to the column removal scenario with self-weight only.
(7) The actuators are extended and placed in contact with the spandrels. The actuator carriages are tightened, and the active push-down loading phase begins.
(8) Load is applied via extension of the vertical actuators at a quasi-static rate. The actuators were daisy-chained together to exert approximately the same force at each actuator. Loading continues monotonically at a quasi-static rate until the downward displacement of the connection zone begins to rapidly increase, indicating a loss of flexural stiffness.

4. Experimental results

The primary goal of these experimental tests is to obtain the relationship between moment at the center of the column and the total rotation at the connection (measured using a tilt meter on the spandrel web near the column face). Since the connection runs through the column and is anchored to adjacent spandrels, the total connection rotation is the sum of the tilt meter rotations measured on both spandrels (i.e. representing the tangential angle between the deflected spandrels where they meet the column). The applied moment is calculated from the load cell data at each actuator using basic equations of static equilibrium. The self-weight moment is included in the computation.

The moment-rotation relationships of both tested connections are plotted in Fig. 8. As expected, the Test 1 connection (with the 1–3/4 in. bars) shows higher moment capacity with less rotational ductility, while the converse (lower moment capacity but greater ductility) is shown during Test 2 (with the 1–3/8 in. bars). The primary events during testing and the moment-rotation milestones at which they occur are summarized in Table 2 and are correspondingly marked on the plotted curves in Fig. 8. During each test, a gap initially opens at the shimmed interface between the bottom anchorage block and the

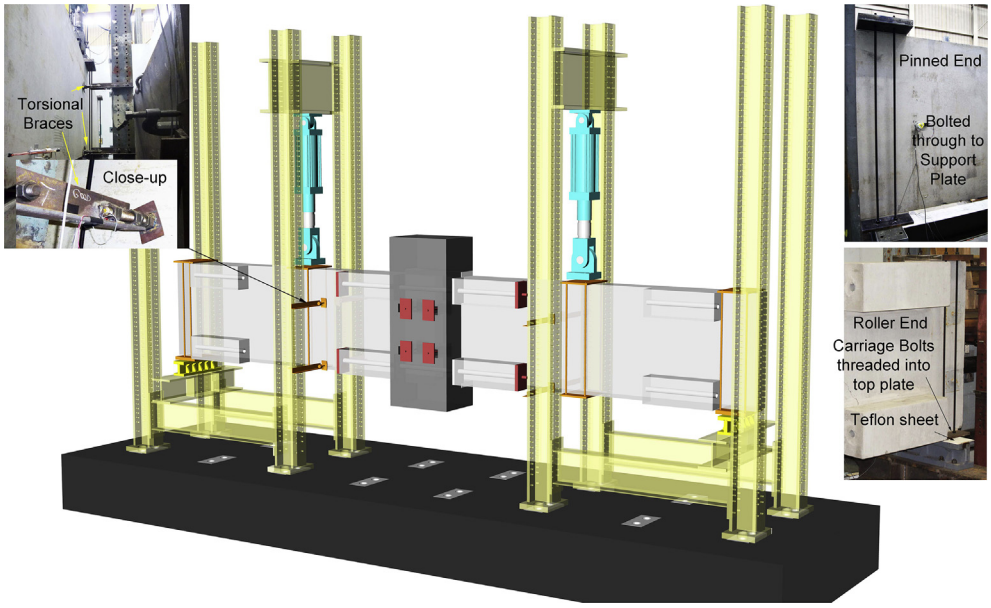

Fig. 6. 3D isometric illustration of the test assembly.

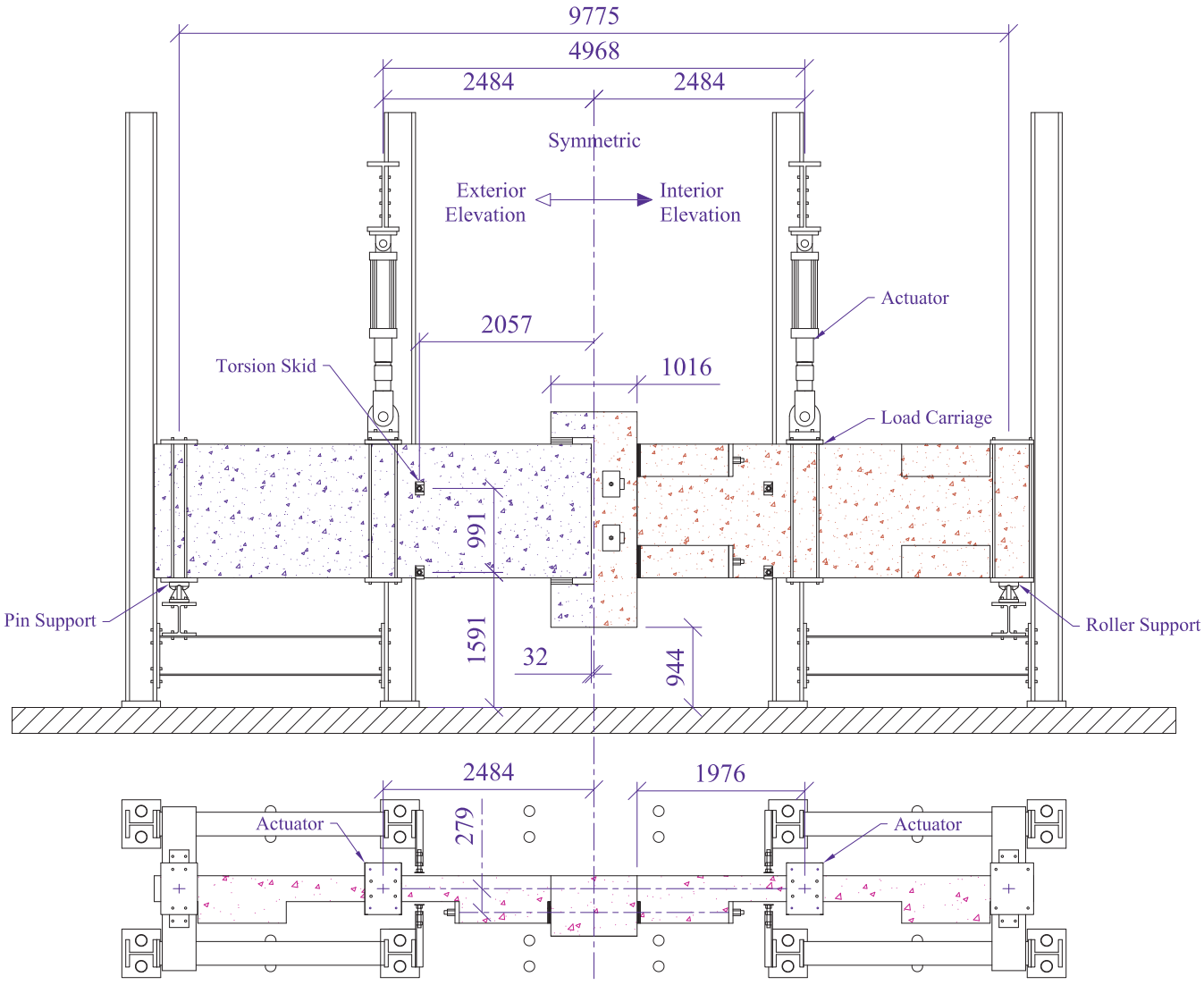

Fig. 7. Test assembly schematic.

Table 1
Predicted connection strengths based on material testing.

Test	Bar area [sq. mm (sq. in.)]	Condition	Bar stress [MPa (ksi)]	Lower bound expected moment [kN-m (kip-ft)]
1	1665 (2.58)	Yield	903.2 (131.0)	1795 (1324)
		Ultimate	1076 (156.1)	2138 (1577)
2	1019 (1.58)	Yield	908.7 (131.8)	1106 (816)
		Ultimate	1085 (157.4)	1321 (974)

column face, followed by the first formation of flexural cracking at the far end of the lower block (Event ID 1). Diagonal cracking then emerges on the interior face of the spandrel in the panel zone between the anchorage blocks (see the post-test photos in Fig. 9). Diagonal cracking also forms on the exterior face of the spandrel in the opposite direction as the interior diagonal cracking. This is attributed to the eccentricity of the load path on the spandrel, which induces a bending moment about the spandrel's vertical axis as the top anchorage block is pushed against the column face and the bottom block is pulled by the anchored through bar under tension. Cracking continues to progress until the through bars yield (Event ID 2), after which plastic rotation accumulates. The yield moments in Fig. 8 correspond to the point at which the strain gauges on the through bars in tension reached the yield strain obtained from the material test results. Yielding and cracking continue until the top anchorage block begins to spall and then crush at its compression contact with the column face (Event ID 3, and also shown in the post-test photos in Fig. 9) – this damage mechanism eventually governs the ultimate failure mode of both connection configurations. After the ultimate moment is reached at Event ID 4, "failure" of the assembly occurs due to a substantial and rapid loss in strength and stiffness until the test is stopped at Event ID 5. Test 1 showed a more significant decrease in moment between Event ID's 4 and 5 than Test 2 due to its larger capacity and thus higher sensitivity to rapid unloading. While some additional capacity may have been available in these subassemblies past Event ID 5, both tests were terminated at this point for safety concerns as the downward deflection and overall cracking began to rapidly increase. Strain gauges on the bars in tension indicated that Tests 1 and 2 utilized approximately 20% and 65%, respectively, of their total strain capacity.

A tilt meter used to monitor the subassembly's column segment for any out-of-plane rotations indicated that the bottom of the column moves towards the front face of the spandrel. This rotation results in an overall tilt of approximately 1.4° when the ultimate in-plane rotation is reached in both tests. Strain gauges monitoring the torsion bars and the axial compression in the torsion skids confirmed this tilt, though strain values in all torsional elements remained very low relative to their strain capacity. Since the spandrels are loaded through their shear centers, the out-of-plane column rotation is primarily caused by the force transfer mechanism through the connection as a result of the 27.9 cm (11 in.) planar eccentricity between the spandrel centerline and the center of the through bars. In an office building, the spandrels are loaded by double-T floor joists resting on corbels that protrude in the same direction as the connection anchorage blocks (see Fig. 2). The flanges of the double-T's are commonly tied to the spandrel with an embedment plate, which would realistically provide restraint to any out-of-plane rotation of the connection assembly.

Photos of the post-test damage are provided in Fig. 9, and a map of post-test crack damage is illustrated in Fig. 10. Cracks on the interior spandrel face are shown with black lines, and red lines are used to represent cracks on the opposing face (i.e. the exterior building face). Together, Figs. 9 and 10 show the opposing diagonal direction of cracking in the spandrel panel zone which began to emerge between Event ID's 1 and 2, as well as the spall and crushing of the top anchorage blocks near their compression interface with the column. During Test 1, the spandrel showed a significant increase in the diagonal cracks as the subassembly approached "failure" – this damage likely contributed to the loss of strength and stiffness at Event ID 5 in combination with the crushing at the top anchorage block. Fig. 10 shows that the column experienced some horizontal cracking and surface spalling during both tests. Post-test inspections of these elements indicated that the surface spall was very shallow and that the cracking severity was relatively minor compared to that shown in the spandrels.

To further evaluate the experimental performance of the connection, Fig. 8 includes horizontal lines for the lower bound expected predictions of yield moment from Table 1 as well as service-level moment and the required design moment in the prototype frame. The service-level demands correspond to unfactored dead plus live (D + L) uniform loading totaling 48.8 kN/m (3.21 kip/ft), which produces a moment at the connection of 326.5 kN-m (240.8 kip-ft). No visible damage was observed in either test at this service-level demand. The required design strength of the spandrel at the support in the prototype building is controlled by the ASCE 7-05 load combination 1.2D + 0.5L + 1.0E (or 1.41D + 0.5L + 1.0Q_E), which results in a factored moment of 971.0 kN-m (716.2 kip-ft). Both tests formed

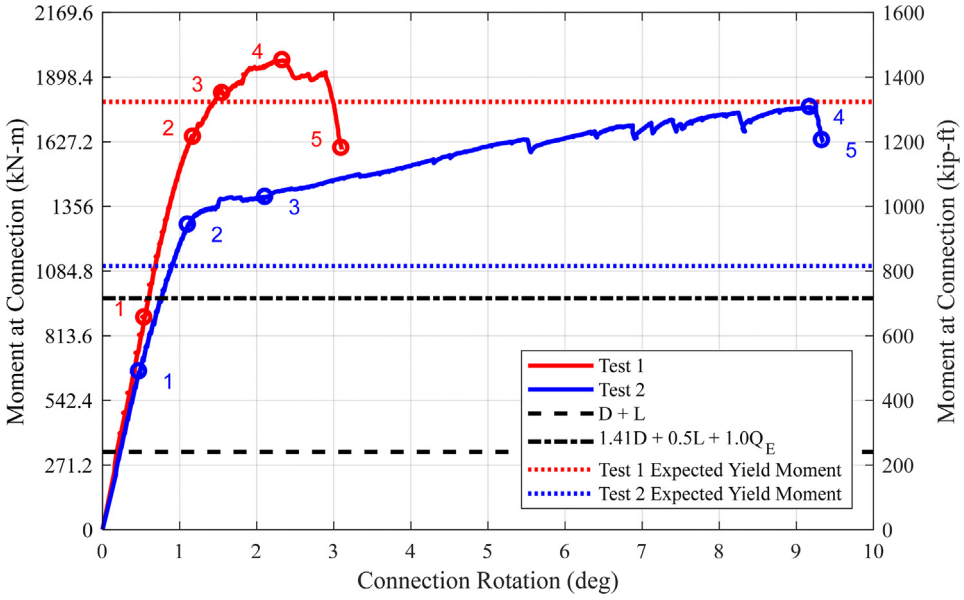

Fig. 8. Measured moment rotation of the tested connections.

Table 2
Events observed during testing.

Event ID	Event description	TEST 1		TEST 2	
		Rotation [deg]	Moment [kN-m (kip-ft)]	Rotation [deg]	Moment [kN-m (kip-ft)]
1	Formation of flexural cracks in spandrel	0.544	889.0 (655.7)	0.477	663.1 (489.1)
2	Yield strain in the through bars is reached	1.18	1653 (1219)	1.11	1276 (941)
3	Crushing initiates at top anchorage block	1.56	1830 (1350)	2.11	1395 (1029)
4	Ultimate moment capacity is reached	2.34	1969 (1452)	9.18	1772 (1307)
5	Termination of test	3.11	1594 (1176)	9.35	1624 (1198)

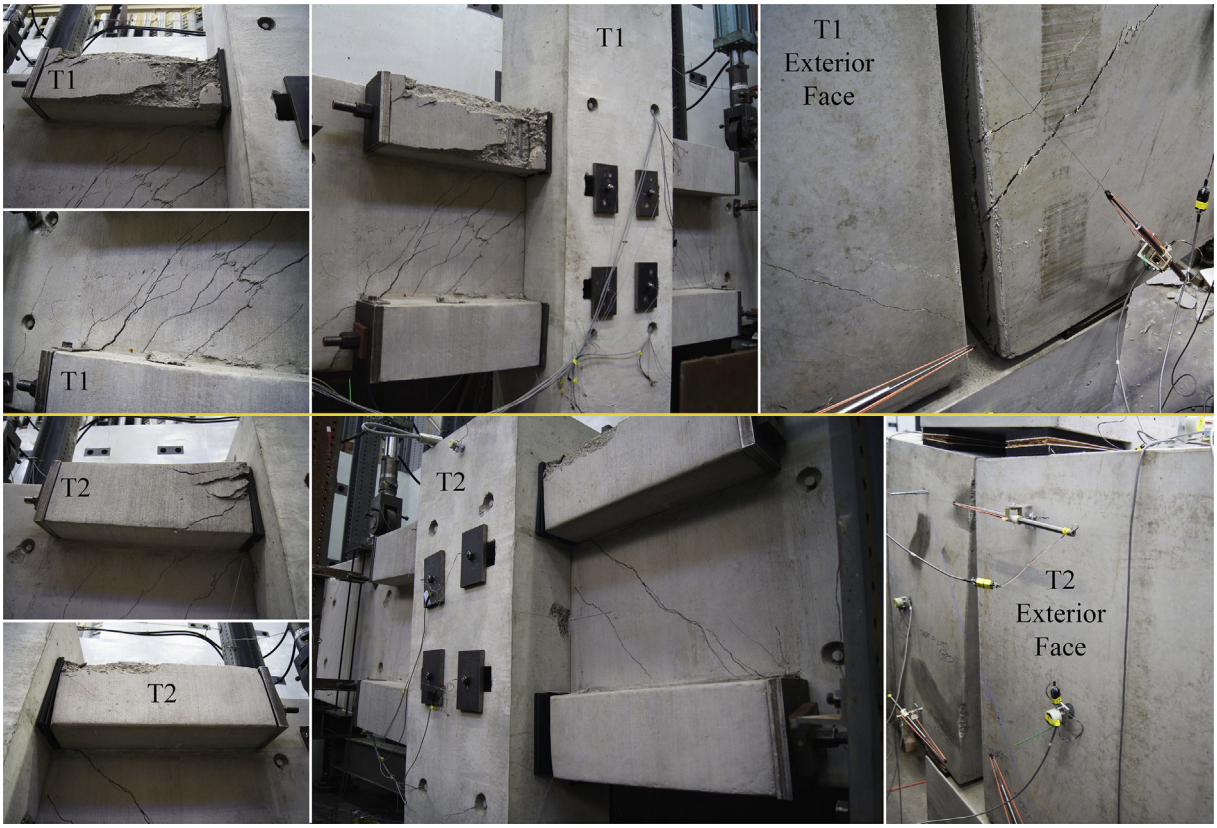

Fig. 9. Post-test damage to the Test 1 and 2 connection specimens.

flexural cracks prior to this load level but did initiate yield until this demand was exceeded.

A summary of predicted and measured moment capacities and rotational deformations is provided in Table 3. As expected, Test 2 showed significantly more rotational deformation capacity (both absolute and relative) when compared with Test 1. In a column removal scenario, the Test 2 connection with the 36 mm (1–3/8 in.) bars would absorb a significant amount of energy through the yielding mechanism as the structure attempts to dynamically reestablish equilibrium. The Test 2 connection was able to comfortably exceed both the lower bound predictions of yield (by 15%) and ultimate moment (by 34%). Recall that the lower bound predictions relied on a rigid body assumption and used a minimum moment arm of 119 cm (47 in.) between the bar locations – the Test 2 results indicate that cracking at larger rotational deformation and a larger moment arm from the tension bar to the compression block may produce a realistically larger capacity. The Test 1 connection with the 46 mm (1–3/4 in.) bars showed yield and ultimate moment capacities that were both 8% lower than the lower bound predicted values. These results indicate that the increased severity of the diagonal cracking due to larger tensile bars forces and overall connection moment (both in-plane and about the vertical axis) may slightly limit the realistic capacity of the subassembly compared to the idealized lower bound predictions.

5. System-level progressive collapse assessment

The experimental moment-rotation relationships were used as input for a system-level modeling assessment of these connections for preventing progressive collapse of the prototype building frame due to a single column removal. SAP2000 Version 17.3 [24] was used to develop a 3D model of the prototype building frame. The analysis is performed via the Nonlinear Dynamic (ND) procedure in accordance with the most recent U.S. Government design standards for progressive collapse resistance [3,4] for a column removal at the first floor, which is the most likely location for removal due to ground-based explosive or impact threats coming from outside the building. The removal scenario considered for this assessment focuses on the column just below the experimental subassembly focus area at location C-1 in Fig. 1. Future research will leverage the results of this study to develop and assess connection strategies for the corner conditions to resist the removal of a column at or adjacent to the corner.

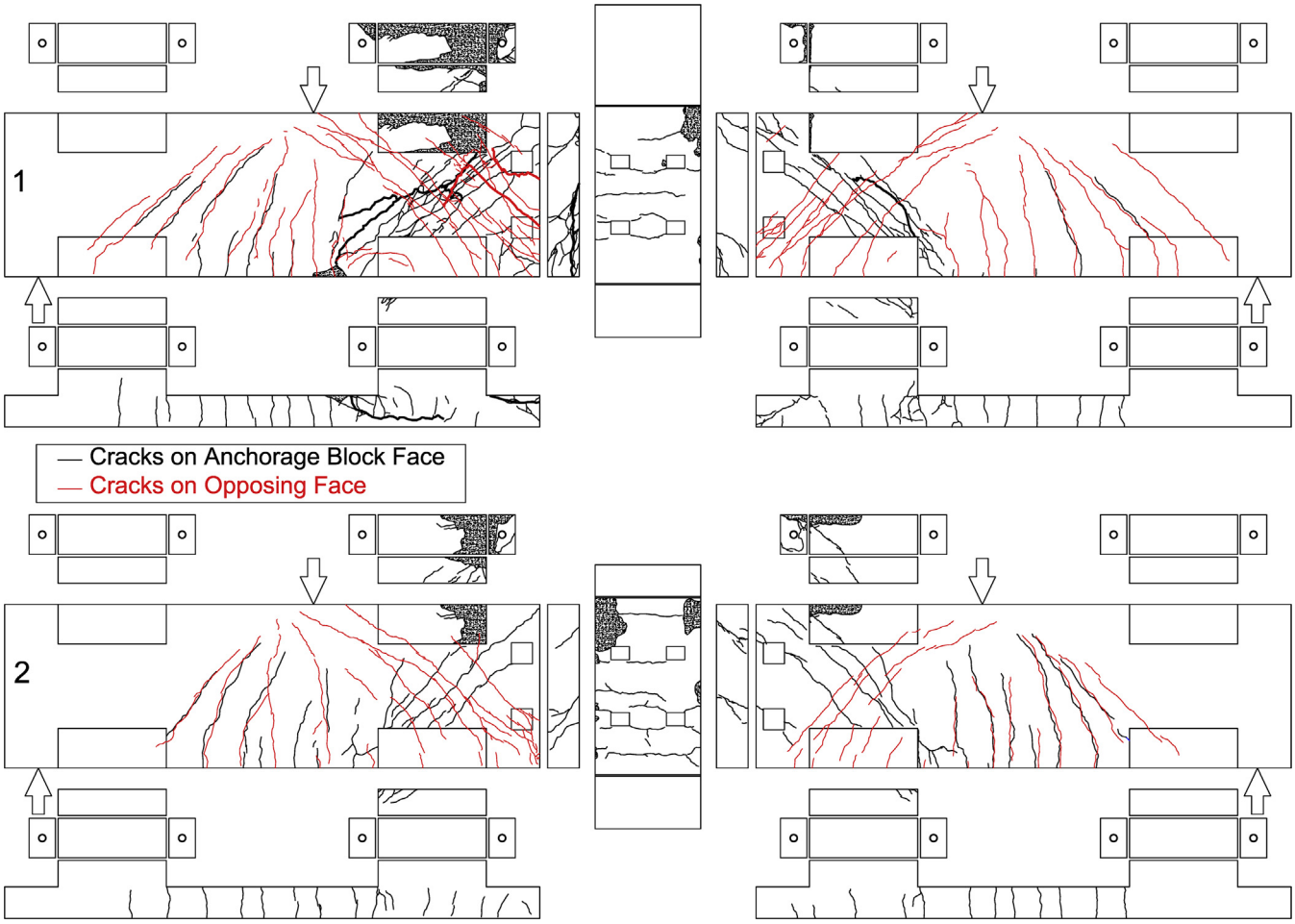

Fig. 10. Illustrations of post-test cracking for Tests 1 and 2.

5.1. Model description

An isometric view of the frame model is shown in Fig. 11. The columns, exterior spandrel girders, interior girders, and the double-T floor joists are modeled with Timoshenko frame elements (i.e. the default option in SAP2000). Each element is modeled with a single frame element between nodal intersections. Preliminary analyses were performed using higher levels of discretization and showed a negligible change in results. The concrete cross-section and reinforcement for each element are input using SAP2000's section designer to obtain realistic flexural response. The section properties for spandrel girders and columns at the perimeter are taken from the schematics shown in Figs. 3 and 4, while those for the interior beams and double-T's are taken from the original prototype design by Kim et al. [15]. Flexural stiffnesses use cracked section properties for their elastic response according to ACI 318 [25]. The potential for nonlinear flexural response beyond the elastic limit is enabled using discrete hinges that are placed at both ends of every frame element on the building perimeter. These hinges account for axial load and moment interaction and are structured according to

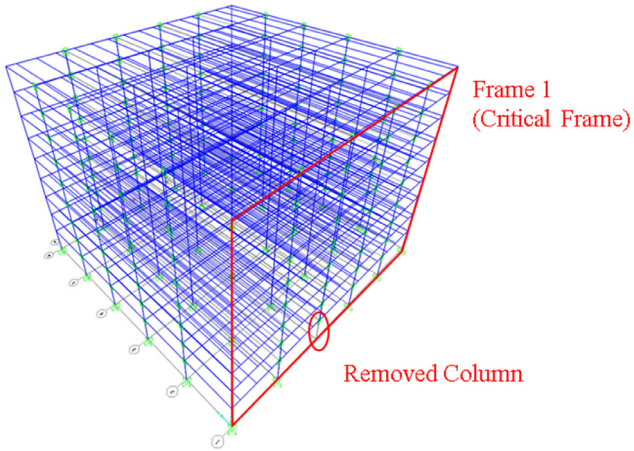

Fig. 11. Numerical model of the prototype building.

Table 3
Comparison of experimental and predicted moment-rotation performance.

Test	Measured					Lower bound expected predictions	
	Yield moment [kN-m (kip-ft)]	Yield rotation [deg]	Ultimate moment [kN-m (kip-ft)]	Ultimate rotation [deg]	Ultimate rotational ductility	Yield moment [kN-m (kip-ft)]	Ultimate moment [kN-m (kip-ft)]
1	1653 (1219)	1.18	1969 (1452)	2.34	2.0	1795 (1324)	2138 (1577)
2	1276 (941)	1.11	1772 (1307)	9.35	8.4	1106 (816)	1321 (974)

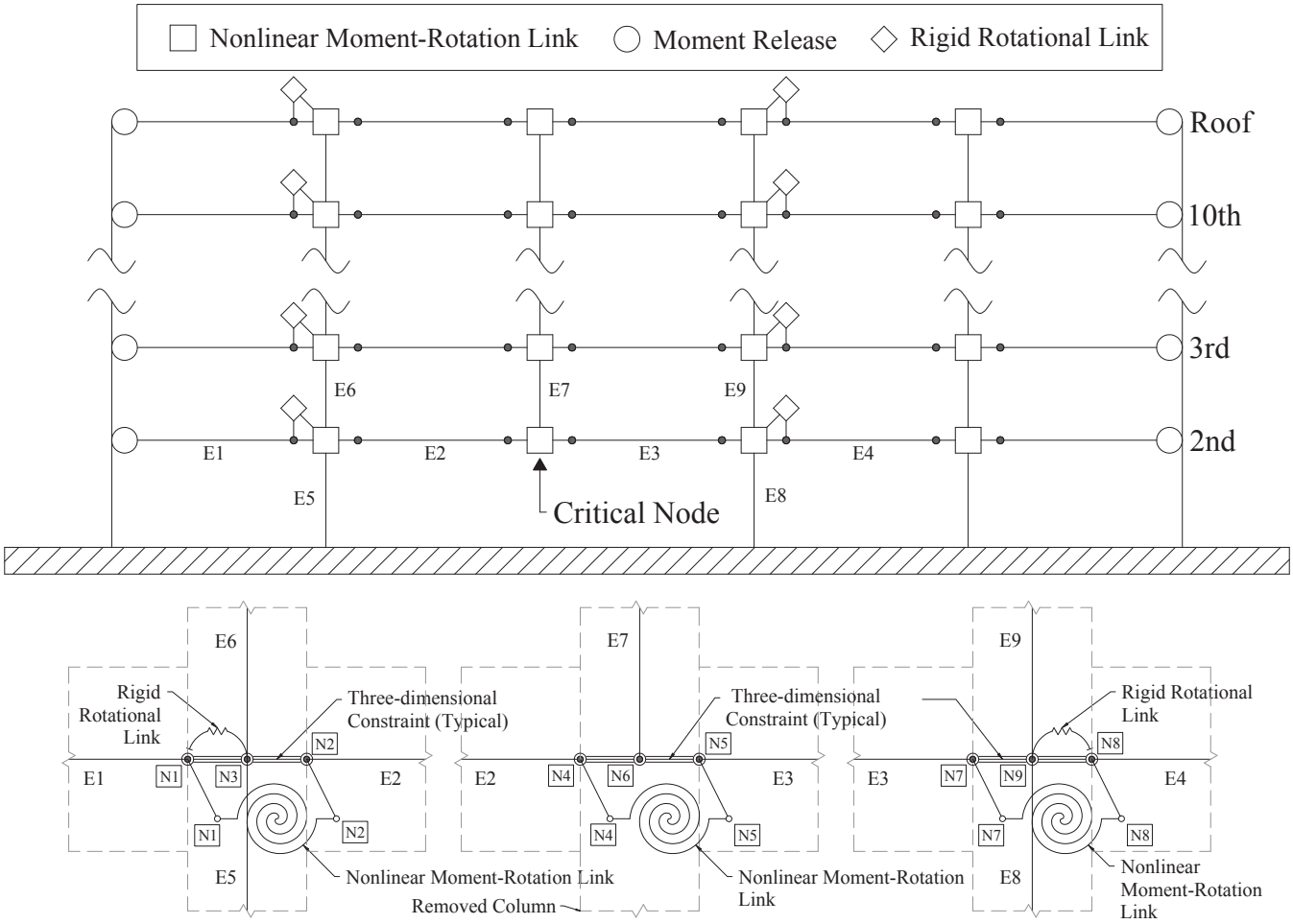

Fig. 12. Critical frame elevation showing the spandrel-to-column connection model.

FEMA 356 [26] using the member properties and section geometry. The bottom of each column at the first floor is conservatively modeled as pinned. A diaphragm condition is defined for each floor to account for the in-plane stiffness of the floor system, as is common practice. All gravity loading is applied to the double-T elements as a line load in accordance with the ASCE 7 extreme load combination (1.2D + 0.5L) using the floor loads specified in Kim et al [15]. It is conservatively assumed that the floor provides no explicit resistance to progressive collapse and simply functions as a load transfer mechanism. The ends of the double-T's are therefore pinned and are not designed to redistribute load via horizontal membrane effects. The interaction of the double-T floor system with the perimeter framing during a progressive collapse scenario is not explicitly modeled and will be considered in future phases of this project.

Fig. 11 highlights the frame along column line 1 as the critical frame for load redistribution when the progressive collapse assessment is conducted for the removal of column C-1 at the ground floor. The moment connections at the spandrel-to-column interfaces are modeled using a combination of rotational link elements and nodal constraints that are illustrated in Fig. 12. The node at each end of a spandrel is offset 50.8 cm (20 in.) from the column centerline to account for the column width. All three translational degrees of freedom at the spandrel end nodes are constrained to (i.e. supported by) the corresponding column node. This accounts for the vertical bearing support, out-of-plane translational restraint via the torsion bars, and longitudinal restraint in bearing against the column. The moment-rotation behavior of the proposed connections are modeled as a nonlinear moment-rotation link element which "passes through" the column (i.e. it is not connected to the column node) to connect the ends nodes of adjacent spandrels, thereby mimicking the connection's through bars.

Prior to the column removal, all spandrel connections will respond in negative bending due to the application of service loads. Under this demand, the connections remain in their elastic range (as shown previously in Fig. 8). When the ground floor column at C-1 is removed, all connections directly above the removal will revert to the positive (and approximately symmetric) flexural response under which the connection was tested, and therefore no further modifications to the connection model shown in Fig. 12 are needed for this location. The connections at the adjacent column lines B and D, however, will respond in negative bending to the column removal. Fig. 12 shows that an additional modification is made to appropriately model the connection in negative bending at the undamaged adjacent columns. The negative flexure developed in the spandrels at the ends of the double bay above the removed column will transfer to the spandrels in the adjacent bay via the unbonded PT bars. This is accomplished with the aforementioned nonlinear moment-rotation link, which bypasses the column to connect the spandrel ends. The spandrels over the column removal (i.e., elements E2 and E3 in Fig. 12) will deflect toward the column removal, and their top anchorage blocks will pull away from the undamaged column at nodes N2 and N7. Conversely, the top anchorage blocks of the spandrels in the adjacent bays (i.e., elements E1 and E4) will bear against the undamaged columns at nodes N1 and N8 due to the transfer of increased negative moment from the E2 and E3 spandrel ends. As shown in Fig. 12, a rigid rotational link element is added between the end nodes of the E1/E4 spandrels (N1 and N8) and the undamaged column nodes (N3 and N9) to allow those spandrels (and their

counterparts at floors above) to impart flexure and shear to the undamaged column due to anchorage block bearing.

5.2. Representing the tested moment-rotation response

To aid numerical convergence of the frame model, the experimental moment-rotation performance of the proposed connection is simplified as a bilinear piecewise function for input to the nonlinear link element. The bilinear curve is developed to produce the same strain energy as the experimentally measured moment rotation. The initial stiffness, k, is determined from linear regression of the elastic range. The maximum moment, M_u, and the rotation at failure, θ_u, from the experiments are used to approximate the final point of the bilinear curve. The area under the experimental moment-rotation curve (A) is calculated from the measured data. The effective yield rotation, θ_y, and moment, M_y, to provide the same strain energy as the experimental test can be calculated utilizing Eq. (1).

$$\theta_y = \frac{2A - M_u \cdot \theta_u}{k \cdot \theta_u - M_u} \tag{1a}$$

$$M_y = k \cdot \theta_y \tag{1b}$$

The bilinear approximations are superimposed onto the experimental moment rotation curves from both tests in Fig. 13. A summary of the yield and ultimate moment-rotation milestones in the bilinear approximations are provided in Table 4.

5.3. Analysis procedure

The ND procedure for progressive collapse analysis [3,4] is used for this assessment because it realistically accounts for both the dynamic amplification of the gravity loads as well as the nonlinear, plastic response of the structure to the column removal scenario [27]. The Nonlinear Static (NS) procedure [3,4] also accounts for plastic structural response but requires a dynamic increase factor (DIF) for loads supported by the removed column to be calculated via provisions in ASCE 41 [28]. The applicable provisions for precast concrete frames are currently under development, however, and a conservative upper bound DIF of 2.0 could instead be used per the current progressive collapse design standards. Using this DIF would overly penalize the resulting assessment of performance, and the NS procedure is therefore not used here.

The ND analyses were performed using an implicit Newmark-Beta direct integration algorithm that included geometric nonlinearity. An initial time step of 5 msec was specified; however, the implicit algorithm in SAP2000 has an adaptive time step to aid numerical convergence. If convergence is not achieved in the specified time step, the increment is subsequently halved until convergence is achieved or a maximum number of iterations is reached, in which case the analysis will terminate.

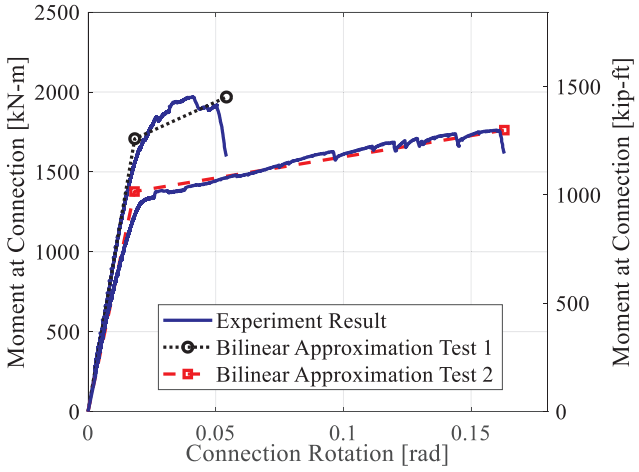

Fig. 13. Bilinear approximation of the experimental moment-rotation connection response.

Table 4
Milestone values in the bilinear approximation of the experimental moment-rotation response.

Test	Yield rotation [rad]	Yield moment [kN-m (kip-ft)]	Ultimate rotation [rad]	Ultimate moment [kN-m (kip-ft)]
1	0.0183	1708 (1260)	0.0542	1969 (1452)
2	0.0183	1385 (1022)	0.1632	1761 (1299)

Before the ND analysis is performed, the undamaged frame is analyzed to obtain the in-situ force and moment due to gravity loads at the top of the column to be removed. Since the structure remains linear under the 1.2D + 0.5L gravity load combination, a linear elastic analysis can be performed to determine these forces. The column of interest is then removed from the model and replaced with these forces and moments as reactions at its top node. Once these forces and the gravity loads have been initialized on the model, the reactions representing the column are quickly removed. A removal time interval must be less than 10% of the natural period of the vertical vibration mode of the damaged structure over the removed column. The response of the frame to this removal characterizes the progressive collapse resistance. Modal analysis of the frame model with the column removed produced values of 0.461 s and 0.502 s for the Test 1 and Test 2 connection links, respectively. A reaction removal interval of 0.04 s was therefore used for both configurations to conform to the 10% limit.

For ND analyses of most reinforced concrete framed systems, damping can typically be taken anywhere from 2 to 5%. However, since the proposed system relies on a non-emulative unbonded post-tensioned force transfer mechanism, damping is likely to be in the lower range and could only be reliably predicted via further dynamic testing. Preliminary analysis using various combinations of mass proportional and stiffness proportional damping, applied either globally to the entire 3D frame or specifically to the removal vibration mode, resulted in a decrease of expected maximum and residual deformation. To be conservative, damping was therefore neglected from the analysis presented here.

Components under high axial load ($P/P_{CL} > 0.5$, where P_{CL} is the lower-bound axial load capacity) are classified as force-controlled. These components, which include the columns, must have a demand-to-capacity ratio less than unity for both combined (1) axial load and biaxial bending and (2) shear. Demand must account for all actions due to ND analysis of the 3D structural model, during which all force-controlled elements are assumed to remain elastic. Capacity for force-controlled elements accounts for lower-bound strength of the material as well as all appropriate strength reduction factors according to the material specific design code. Components with low axial load ($P/P_{CL} \leq 0.5$) such as the spandrels and their connections are classified as deformation-controlled and are modeled as capable of plastic deformation. Plastic moment capacity and rotational limits of deformation-controlled elements account for the expected strength of the material.

5.4. Analysis results

Results of ND analysis for the first-floor column removal at C-1 using both the bilinear Test 1 and Test 2 connection link configurations showed that both connections were able to successfully prevent progressive collapse of the frame. Nonlinear flexural behavior in both cases was confined to the connection links in keeping with their design intent as a structural “fuse” – no nonlinear hinge behavior emerged in the

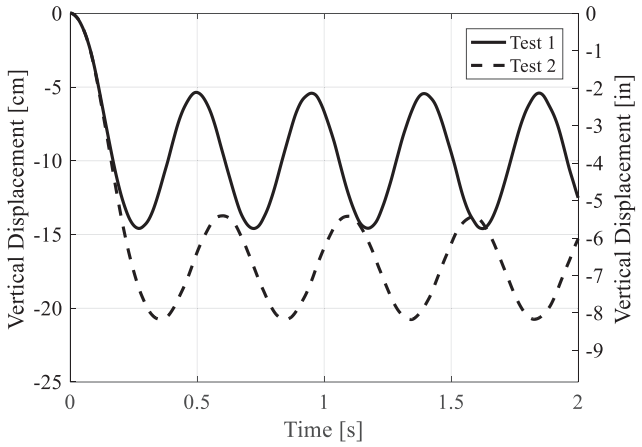

Fig. 14. Time histories of vertical displacement just above the column removal.

spandrel elements themselves. Time histories of the vertical displacement of the node directly above the removed column are plotted in Fig. 14. The frame experienced large deflections of just under 15 cm for Test 1 and slightly more than 20 cm for Test 2 when the column was suddenly removed in both analyses and subsequently achieved a stable state of free vibration.

The nonlinear capacity utilization (NCU) of every connection link in the critical frame in Figs. 11 and 12 is calculated according to Eq. (2) as a measure of the maximum nonlinear deformation from ND analysis relative to the available nonlinear deformation capacity of the connection between yield and ultimate.

$$NCU = (100\%) * \frac{|\theta_{max}| - \theta_y}{\theta_u - \theta_y} \tag{2}$$

A distributed plot of all NCU values in Fig. 15 shows that the maximum values just exceeded 40% and 20% of the available nonlinear capacity for the Test 1 and Test 2 connections, respectively. The frame with Test 1 connections experienced a larger dynamic amplification of its gravity loads due to the larger stiffness and capacity of the connection, and the nonlinear behavior was confined to the midspan connections. Conversely, the frame with the more ductile Test 2 connections experienced lower dynamic amplification of gravity loads and developed a wider distribution of nonlinear response. Though both connections were effective in resisting progressive collapse, the ductility of the Test 2 connection mitigates the dynamic load amplification and can offer significant resistance with a lower moment-rotation ultimate capacity.

As shown in Fig. 15, the connection link elements in the second floor 2-bay span directly above the removed column experienced the largest moment-rotation deformations during the ND analyses. The time history hysteresis of the connection links at the midspan (positive bending) and end (negative bending) of the 2-bay span are plotted in Figs. 16 and 17 for Test 1 and Test 2, respectively. As shown, the critical link elements have not exceeded their respective ultimate capacity state in either of the two analyses. Both connections in the Test 2 configuration have yielded, though only the midspan connection has yielded in the Test 1 configuration. The elastic unloading shown in these figures occurs after the first peak response to the column removal, and no further permanent rotation is incurred during the subsequent undamped sinusoidal vibrations.

Immediately following the column removal, the load in the remaining undamaged columns above the removal (above the second floor at C-1) decreases rapidly from its original in-situ state to a negligible value and then oscillates near zero due to undamped vibration. The post-removal bending moment in those columns is also negligible. This occurs because the same spandrel and connection are used over the height and width of the building perimeter, thereby distributing progressive collapse resistance almost equally to each floor in an approximately symmetric pattern as demonstrated in Fig. 15. Conversely, the adjacent undamaged columns at locations B-1 and D-1 experience a rapid increase of axial load and moment due to load redistribution from the removed column. The columns at B-1 and D-1 are classified as force-controlled elements due to their high P/P_{CL} ratio, and therefore the peak demand from ND analysis for combined axial load and moment as well as shear is checked against the factored lower bound capacity according to ACI 318 [25]. Fig. 18 shows that the maximum combinations of axial load and moment experienced by the columns at locations B-1 and D-1 exceeded the factored capacity envelope for the as-built pocketed (i.e. minimum) column section shown in Fig. 4 with concrete strength of 41.4 MPa (6 ksi). A new capacity envelope which successfully meets the maximum demand is developed by increasing the concrete strength to 68.9 MPa (10 ksi) and decreasing the width dimension of the torsion bar blockouts by half. These modifications could be easily accommodated in practice – concrete strengths in this range are easily attainable in precast element fabrication, and the as-built width of the torsion bar blockouts was not fully utilized in either of the experimental tests. The maximum shear demand reached only 66% and 56% of the available shear capacity of the as-built pocket column section for the Test 1 and 2 connection configurations, respectively.

6. Conclusions

A novel exterior spandrel-to-column moment connection detail for progressive collapse resistant precast concrete building frames was developed and examined experimentally and then implemented in a system-level model. The experimental subassembly was fabricated at full scale and evaluated through destructive testing. The connection is non-emulative and utilizes unbonded high-strength steel post-tensioning (PT) bars which pass through ducts in the column and are anchored to the spandrels via bearing plates. Two PT bar sizes with 1034 MPa (150 ksi) nominal ultimate strength are examined: a larger diameter bar (46 mm (1–3/4 in.)) is used to evaluate a higher strength, lower ductility connection; and a smaller diameter bar (36 mm (1–3/8 in.)) is used to examine a lower strength, higher ductility condition. The experimental results are used to numerically assess the progressive collapse resistance of a prototype 10-story precast concrete office building. The following conclusions can be made:

- No visible damage was observed in either tested connection under service level loads. Both tests formed flexural cracks prior to reaching the required design strength but did not initiate yield until this demand was exceeded.
- Distributed cracking of the spandrels was observed as the PT bars yielded and the connections progressed toward their ultimate moment-rotation. Spalling and eventual crushing at the top anchorage block in contact with the column face eventually governed the ultimate failure mode of both connection configurations.
- The smaller bar configuration showed three times more rotational deformation capacity vs. the larger bar configuration. The larger bar configuration only showed 12% higher ultimate strength than the smaller bar configuration.
- A lower bound estimate of yield and ultimate moment capacity was calculated for each connection using simplified rigid body assumptions and taking the moment arm at the connection between the bars. The smaller bar configuration was able to comfortably exceed lower bound predictions of both yield (by 15%) and ultimate moment (by 34%). The larger bar configuration showed yield and ultimate moment capacities that were both 8% lower than the lower bound predicted values. This approach can be useful for achieving a conservative design.
- Both configurations showed diagonal cracking due to the in-plane eccentricity between the applied vertical load (above the spandrel centerline), the PT bars in tension, and the compression at the top

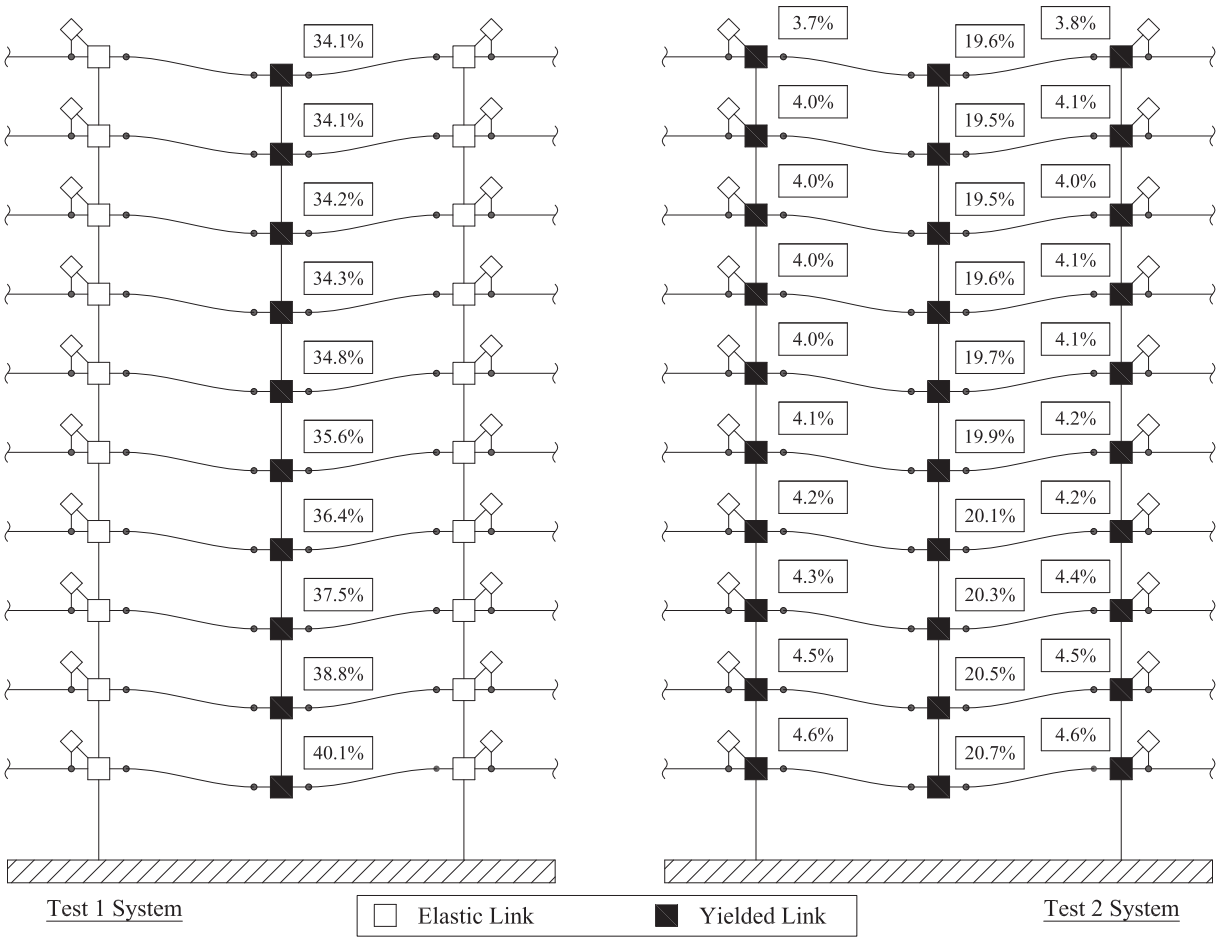

Fig. 15. NCU values in the critical frame (shown as representatively deformed) due to the peak results of ND analysis.

anchorage block. The load path in the anchorage region relative to realistic floor loading (applied at corbels on the interior spandrel face) should be investigated further to minimize these complex cracking mechanisms.

- Bilinear moment-rotation resistance functions were developed from the experimental results and input into a nonlinear dynamic progressive collapse analysis of the prototype 10-story office building. Results showed that both connections are capable of arresting progressive collapse of the building when subject to the loss of a first floor column. At the locations of maximum ductility, the larger and smaller bar configurations just exceeded 40% and 20% of their available nonlinear capacity, respectively.
- Though both connections were effective in resisting progressive collapse, the ductility of the smaller bar configuration mitigates the dynamic load amplification and can offer adequate resistance at a lower moment-rotation ultimate capacity.
- The progressive collapse analyses indicated that the adjacent undamaged columns in the perimeter frame can experience P-M overload as a result of the removal scenarios in their as-built prototype configuration. This issue can be readily addressed by using higher strength concrete for these elements and decreasing the size of the torsion bar blockouts (which were underutilized in the experimental tests).

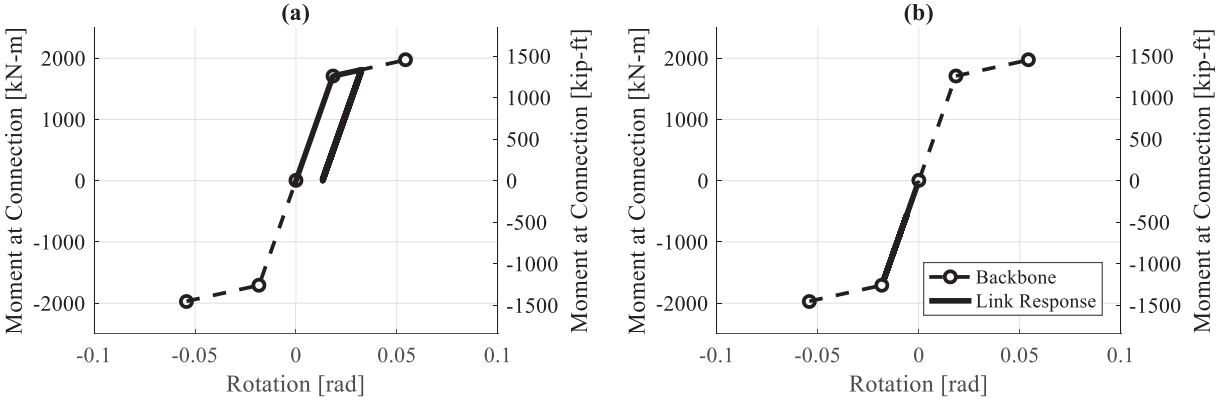

Fig. 16. Response of the Test 1 connection links in the span directly above the removed column: (a) midspan and (b) end.

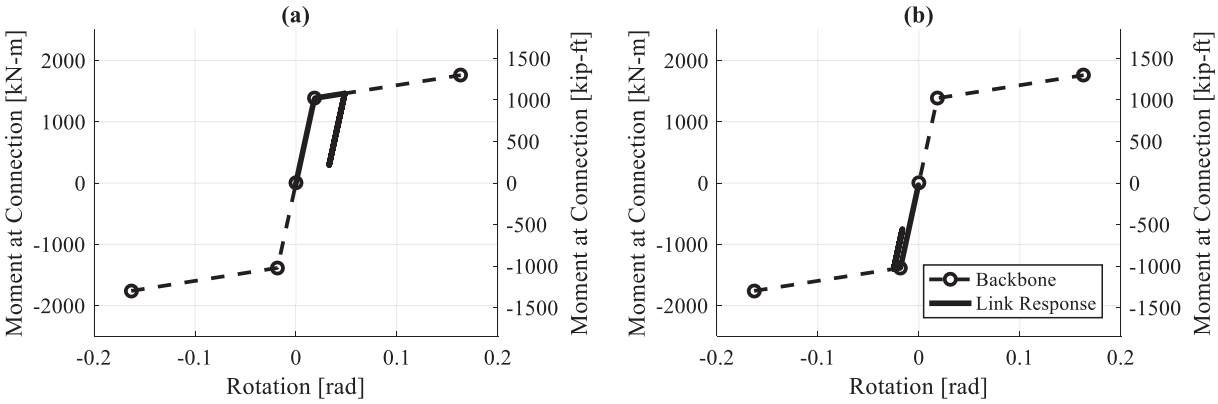

Fig. 17. Response of the Test 2 connection links in the span directly above the removed column: (a) midspan and (b) end.

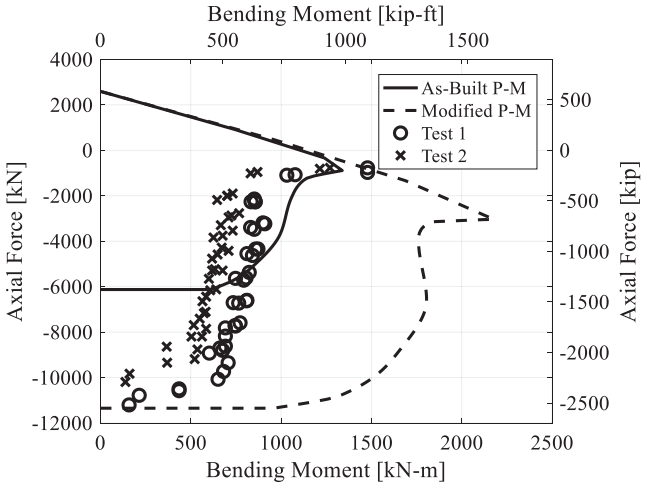

Fig. 18. Column axial force vs. bending moment capacity at maximum ND demand.

Acknowledgements

This project is supported by the Precast/Prestressed Concrete Institute (PCI) via the Daniel P. Jenny Fellowship (2014) and by the Pennsylvania Infrastructure Technology Alliance (PITA). In addition, the following companies graciously donated labor, materials and transportation of subassembly components and testing equipment: Metromont Corporation, J.R. Slaw, Inc., Williams Form Engineering Corp., Meadow Burke, and JVI, Inc. The testing was conducted at Lehigh University's Advanced Technology for Large Structural Systems (ATLSS) Engineering Research Center. The authors would like to sincerely thank all groups and companies involved throughout this project – their generosity and guidance has been invaluable. The authors would like to specifically thank Roger Becker of PCI for his guidance and insight throughout this research effort.

References

[1] Pearson C, Delatte N. Ronan point apartment tower collapse and its effect on building codes. J Perform Constr Facil 2005;19:172–7. https://doi.org/10.1061/(ASCE)0887-3828(2005) 19:2(172).
[2] Corley WG, Mlakar PF, Sozen MA, Thornton CH. The Oklahoma City Bombing: summary and recommendations for multihazard mitigation. J Perform Constr Facil 1998;12:100–12. https://doi.org/10.1061/(ASCE)0887-3828(1998)12:3(100).
[3] DoD. Design of buildings to resist progressive collapse (Change 3). UFC 4-023-03; 2016.
[4] GSA. Alternate path analysis & design guidelines for progressive collapse resistance (Rev. 1). Washington, DC: General Services Administration; 2016.
[5] Burns J, Abruzzo J, Tamaro M. Structural systems for progressive collapse prevention. Multihazard Mitig. Counc. Natl. Work. Prev. Progressive Collapse, Chicago, IL. 2002. p. 1–5.
[6] DoD. DoD Security Engineering Facilities Planning Manual. UFC 4-020-01; 2008.
[7] Precast/Prestressed Concrete Institute. PCI Design Handbook. 7th ed. Chicago, IL; 2010.
[8] Regan PE. Catenary tests on composite precast–in situ concrete composite floors. London, UK: Report to the Department of Environment; 1974.
[9] Fintel M, Schultz D. Structural integrity of large panel buildings. ACI J 1979:583–620.
[10] Enstock LK, Smith PD. Measurement of impulse from the close-in explosion of doped charges using a pendulum. Int J Impact Eng 2007;34:487–94. https://doi.org/10.1016/j.ijimpeng.2005.12.005.
[11] Kang SB, Tan KH. Behaviour of precast concrete beam-column sub-assemblages subject to column removal. Eng Struct 2015;93:85–96. https://doi.org/10.1016/j.engstruct.2015.03.027.
[12] Nimse RB, Joshi DD, Patel PV. Behavior of wet precast beam column connections under progressive collapse scenario: an experimental study. Int J Adv Struct Eng 2014;6:149–59. https://doi.org/10.1007/s40091-014-0072-3.
[13] Nimse RB, Joshi DD, Patel PV. Experimental study on precast beam column connections constructed using RC corbel and steel billet under progressive collapse scenario. Struct. Congr. 2015. 2015. p. 2089–100.
[14] Main JA, Bao Y, Lew HS, Sadek F, Chiarito VP, Robert SD, et al. An experimental and computational study of precast concrete moment frames under a column removal scenario. Gaithersburg, MD: National Institute of Standards and Technology; 2015. https://doi.org/10.6028/NIST.TN.1886.
[15] Kim J, Dasgupta P, Ghosh SK. Assessment of the ability of seismic structural system to withstand progressive collapse – design of precast concrete frame building (Seismic Design Category D). Palatine, IL; 2009. https://www.skghoshassociates.com/reports/ [accessed 9/2018].
[16] ASCE. ASCE 7–05: Minimum design loads for buildings and other structures. Reston, VA: American Society of Civil Engineers; 2005.
[17] ACI. Building code requirements for structural concrete (ACI 318-05) and commentary (ACI 18R-05). Farmington Hills, MI; 2005.
[18] PCI. PCI Design Handbook. 6th ed. Chicago, IL; 2004.
[19] ASTM. A722: Standard specification for uncoated high-strength steel bars for prestressing. vol. 1; 2015.
[20] ASCE. ASCE 7–16: Minimum design loads for buildings and other structures. Reston, VA: American Society of Civil Engineers; 2016.
[21] Quiel S, Naito C, Fallon C. ATLSS Report 16-08: Experimental evaluation of a new moment connection for progressive collapse resistant precast concrete frames. Bethlehem, PA; 2017. https://doi.org/10.13140/RG.2.2.28215.62884.
[22] ASTM. C39: Standard test method for compressive strength of cylindrical concrete specimens; 2014.
[23] ASTM. A370: Standard test methods and definitions for mechanical testing of steel products; 2014.
[24] CSI. SAP2000 Ultimate, Version 17.3; 2015.
[25] ACI. Building code requirements for structural concrete (ACI 318-14) and commentary (ACI 318R-14). Farmington Hills, MI; 2014.
[26] FEMA. Prestandard and commentary for the seismic rehabilitation of buildings (356). Washington, DC: Federal Emergency Management Agency; 2000.
[27] Marjanishvili SM, Agnew E. Comparison of various procedures for progressive collapse analysis. J Perform Constr Facil 2006;20:365–74. https://doi.org/10.1061/(ASCE)0887-3828(2006)20:4(365).
[28] ASCE. Seismic evaluation and retrofit of existing buildings (41-17). Reston, VA: American Society of Civil Engineers; 2017.